Colored object encoding scheme in ghost imaging system using orbital angular momentum

Yongqiang Li (李永强), Hua Yang (杨 华), Jiao Liu (刘 娇), Longyan Gong (巩龙奕), Yubo Sheng (盛宇波), Weiwen Cheng (程维文), and Shengmei Zhao (赵生妹)*

Institute of Signal Processing and Transmission, Nanjing University of Posts and Telecommunications, Nanjing 210003, China

**Corresponding author: zhaosm@njupt.edu.cn*

Received June 18, 2012; accepted August 13, 2012; posted online January 21, 2013

A colored object encoding scheme in a ghost imaging (GI) system using orbital angular momentum is investigated. A colored object is decomposed into three components and then each component is obtained in the idler arm using a multiple grayscale encoding scheme. Afterward, we synthesize the three reconstructed components into a colored image. The scheme is conducted and then presented through numerical simulations and experiments. The simulation result shows that the average peak signal-to-noise ratio (PSNR) is at 21.636 for the reconstructed color of the "Lena" image with 255 gray scales. The experiment also shows that the PSNR is 8.082 for the reconstructed color of the "NUPT" characters. The successful imaging of colored objects extends the further use of the GI technique.

OCIS codes: 110.1650, 070.6120, 270.0270.
doi: 10.3788/COL201311.021104.

Ghost imaging (GI), also known as coincidence imaging, is a novel imaging technique that has become increasingly popular over the last decade[1−4]. In this system, photons are spatially separated and propagated along a distinct optical path. The path including object is usually called the "signal arm," and the other one is named the "idler arm." The intensity correlation between the signal beam, which encounters the target, and the idler beam, which impinges on the high spatial resolution detector, imparts the information of the target into the idler arm. This phenomenon is named GI. The GI technique offers great potential with regard to standard imaging. The technique allows the imaging of objects that are located in optically harsh or noisy environment, such as in military, astronomical, and medical X-ray imaging fields. Recently, the GI technique has been reported to be applicable in wireless communication technologies[5].

The GI technique was first demonstrated by utilizing a biphoton source to entangle source photons[6]. Subsequently, theoretical[7,8] and experimental[9−11] works demonstrated that GI can be performed using pseudo-thermal light or true thermal light[12,13]. Other studies regarding GI include computational GI[14,15], compressive GI[16], differential GI[12,17], and reflective GI[18,19]. Recently, Jack *et al*. implemented holographic GI (HGI) using orbital angular momentum (OAM), whereby the contrast of the edge imaging is enhanced[20]. The OAM state with one photon carries more than one bit of information compared with the polarization state encoded in the polarization degrees of freedom. A multiple grayscale encoding scheme with OAM was proposed according to the strong time and spatial correlation of entangled photons[20−22]. In this scheme, different grayscales are represented by different phase matrixes. This development has led to the possibility of presenting GI for colored objects. Compared with grayscale objects, colored objects have more information and provide better data for object recognition. In this letter, we investigate a GI scheme for colored objects using OAM.

In holographic GI systems, the mode of the pump, signal, and idler can be described by normalized transverse mode functions: $\Phi_{(\vec{x}_i)}$ (i=s, i, p), where $\vec{x}$ is a vector in the plane perpendicular to the propagation direction of light, and subscripts p, s, and i denote the pump, signal, and idler beam, respectively. The two-photon wave function of the signal and idler generated by spontaneous parametric down-conversion (SPDC)[23,24] is expressed as

$$|\psi\rangle = \int \mathrm{d}\vec{k}_\mathrm{p} \int \mathrm{d}\vec{k}_\mathrm{s} \int \mathrm{d}\vec{k}_\mathrm{i} \Phi_\mathrm{p}(\vec{k}_\mathrm{p}) \widehat{a}_\mathrm{i}^{+}(\vec{k}_\mathrm{i}) \widehat{a}_\mathrm{s}^{+}(\vec{k}_\mathrm{s}) \times \Delta(\vec{k}_\mathrm{s} - \vec{k}_\mathrm{i}) \delta^{(2)}(\vec{k}_\mathrm{p} - \vec{k}_\mathrm{s} - \vec{k}_\mathrm{i}) \, |0\rangle \,, \tag{1}$$

where $\widehat{a}^{+}$ is the creation operator, $|0\rangle$ is the initial vacuum state, k is the transverse component of the mode function wave vector, $\Phi_\mathrm{p}(k)$ is the Fourier transformation of the transverse function, $\delta^{(2)}$ is the two-dimensional (2D) delta function, and $\Delta(\cdot)$ is the pure geometrical function. Through Fourier transformation, Eq. (1) is written as

$$|\psi\rangle = \int \mathrm{d}\vec{x}_\mathrm{s} \int \mathrm{d}\vec{x}_\mathrm{i} \Phi_\mathrm{p}\Big(\frac{\vec{x}_\mathrm{s} + \vec{x}_\mathrm{i}}{2}\Big) \cdot \Delta(\vec{x}_\mathrm{s} - \vec{x}_\mathrm{i}) \widehat{a}_\mathrm{s}^{+}(\vec{x}_\mathrm{s}) a_\mathrm{i}^{+}(\vec{x}_\mathrm{i}) \, |0\rangle \,. \tag{2}$$

The coincidence probability of photons both in the signal mode Φ_s and the idler mode Φ_i is then expressed by

$$P(\Phi_\mathrm{s}, \Phi_\mathrm{i}) = [\langle \psi_\mathrm{i}, \psi_\mathrm{s} | \psi \rangle]^2 = \Big[\int \mathrm{d}\vec{x}_\mathrm{s} \int \mathrm{d}\vec{x}_\mathrm{i} \Phi_\mathrm{s}^{*}(\vec{x}_\mathrm{s}) \Phi_\mathrm{i}^{*}(\vec{x}_\mathrm{i}) \cdot \Phi\Big(\frac{\vec{x}_\mathrm{s} + \vec{x}_\mathrm{i}}{2}\Big) \Delta(\vec{x}_\mathrm{s} - \vec{x}_\mathrm{i}) \Big]^2 . \tag{3}$$

For normalized Laguerre-Gaussian modes, the transverse

mode function is described as

$$\Phi_{m,n}(r,\varphi)=|n\rangle=\sqrt{\frac{2m!}{\pi(|n|+m)!}}\cdot\sqrt{\frac{1}{w}}\left(\frac{r\sqrt{2}}{w}\right)^{|n|}L_m^{|n|}\left(\frac{2r^2}{w^2}\right)\mathrm{e}^{-r^2/w^2}\mathrm{e}^{-\mathrm{i}n\varphi}, \tag{4}$$

where $L_m^{|n|}$ is the generalized Laguerre polynomial; n and m are the radial and azimuthal mode indices, respectively; r is the radial cylindrical coordinate; w is the beam waist; and φ is the azimuthal angle. The normalized coincidence probability results in the insertion of spatial mode function Eq. (4) in Eq. (3). Hence, we have

$$p_{\mathrm{N}}(\Phi_{\mathrm{s}},\Phi_{\mathrm{i}})=\sin c^2[(l_{\mathrm{s}}+l_{\mathrm{i}}-l_{\mathrm{p}})\pi]\frac{|R_{\mathrm{si}}|^2}{\sqrt{R_{\mathrm{s}}R_{\mathrm{i}}}}, \tag{5}$$

where R_{si}, R_{s}, and R_{i} are the computational constants; and N represents the normalized coincidence probability. The result shows that the coincidence rate obtains the maximum value if the OAM is conserved. However, the coincidence rate vanishes if $l_{\mathrm{s}}+l_{\mathrm{i}}-l_{\mathrm{p}}$ is a nonzero integer. Therefore, if a sector state $|\theta_{\mathrm{A}}\rangle$ is set at the signal arm and another sector state $|\theta_{\mathrm{B}}\rangle$ is set at the idler arm, the coincidence probability with $l_{\mathrm{p}}=0$ is expressed as

$$C(\theta_{\mathrm{A}},\theta_{\mathrm{B}})=|\langle\theta_A|\langle\theta_{\mathrm{B}}|\,|\psi\rangle|^2\propto\cos^2[l(\theta_{\mathrm{A}}-\theta_{\mathrm{B}})]. \tag{6}$$

Here, the sector state $|\theta\rangle$ is defined as the superpositions $|+l\rangle$ and $|-l\rangle$ with an arbitrary relative phase, which expressed as

$$|\theta\rangle=\frac{1}{\sqrt{2}}(\mathrm{e}^{\mathrm{i}l\theta}\,|+l\rangle+\mathrm{e}^{-\mathrm{i}l\theta}\,|-l\rangle), \tag{7}$$

where the angle θ relates to the orientation of the sector state. Furthermore, different coincidence rates can be obtained from Eq. (6) if different sector states $|\theta_{\mathrm{A}}\rangle$ are used to represent the different grayscales of the object while keeping $|\theta_{\mathrm{B}}\rangle$ constant. A GI scheme for colored objects is thus proposed based on this relationship.

A colored object is a special multi-spectral image that corresponds to the three primary colors of human vision: red (R), green (G), and blue (B)[25]. Each pixel of a colored image can be decomposed into the three components of RGB. Thus, an image of a colored object can be synthesized by using multiple grayscale GI encoding for each component. The schematic setup of a colored object for HGI is shown in Fig. 1.

The information of the colored object in the signal arm is decomposed into three components: R, G, and B. Afterwards, different sector states ($\theta\in[0,\ \pi/2]$) with l=1 are selected to represent the grayscale information in each component. For example, the orientations of the sector state θ may be selected as 0, $\pi/2M$, $2\pi/2M$, or $(M–1)\pi/M$ for M different gray scale values. A Hermite-Gaussian mode $\mathrm{HG}_{+1,0}$[26], which is actually the sector state with θ=0, is assigned to the idler beam. All sector states in the experiment are modulated toward the beam by a spatial light modulator (SLM). According to Eq. (6), the coincidence rates will be different for different sector states in a signal beam. The grayscale information of the object in the idler arm can be recovered by post processing the coincidence rate. Then, the color images in the idler arm can be synthesized after the three reconstructed components are obtained. The most common representation, such as RGB, is used to represent a colored image. The colored spaces of the RGB can be stored in different ways according to the different processing power of the device[25]. The present study used the 24-bit implementation, that is, the RGB channel occupies 8 bits each. In principle, the colored space model illustrates a 256×256×256≈1 670 million kinds of colors on this 24-bit RGB.

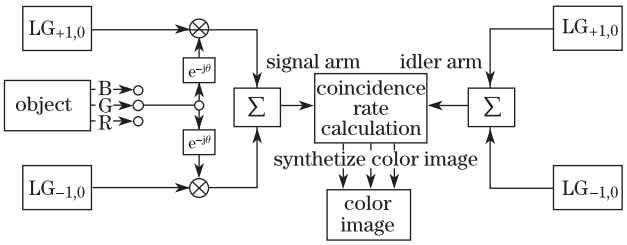

Fig. 1. Schematic setup of a colored object for HGI.

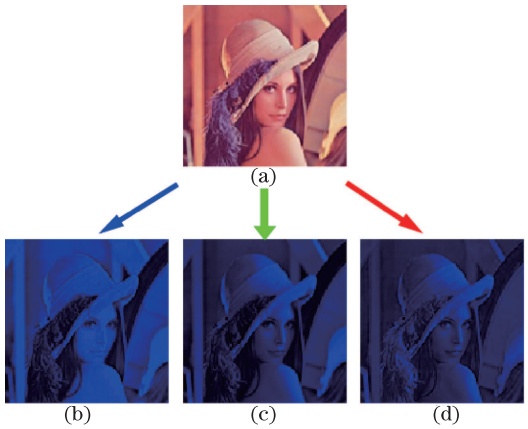

Fig. 2. (a) RGB color image, (b) B component image, (c) G component image, and (d) R component image.

The scheme is first implemented through numerical simulation. A color "Lena" image, which has 128×128 pixels with 255 gray scales, is used for the numerical experiment. The colored image of the object in the signal arm is decomposed into three components: R, G, and B component. Each pixel is described by a 24-bit space in the colored object representation: the first 8-bit space is B, the middle 8-bit space is G, and the last 8-bit space is R. Every first 8-bit is distilled from each pixel of the colored image to compose the B , R, and G components The original colored "Lena" object and its RGB components are shown in Fig. 2. After the decomposition, the proposed schemes for the colored object are used to obtain each image of the component in the idler arm. A total of 255 sector states are thus selected in the signal to represent the grayscale information of each component.

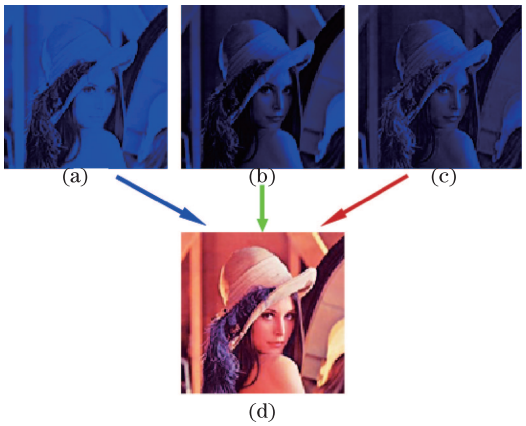

Fig. 3. (a) Result of B channel GI simulation: PSNR= 20.3564; (b) result of G channel GI simulation: PSNR= 22.4585; (c) result of R channel GI simulation: PSNR= 22.0929; (d) color image simulation of GI: PSNR= 21.636.

The reconstructed image of the colored object using the proposed scheme is shown in Fig. 3. Finally, the colored image is recovered by synthesizing the three reconstructed components from the GI system using multiple grayscale encoding. The colored "Lena" image is recovered correctly and accurately using the proposed scheme, as shown in Fig. 3(d).

The peak signal-to-noise ratio (PSNR) is used to evaluate and quantify the recovered image from the GI system objectively. The PSNR is defined as

$$\mathrm{PSNR} = 10\lg\frac{(\mathrm{maxvalue})^2}{\frac{1}{N^2}\sum[a(x,y)-b(x,y)]^2}, \qquad (8)$$

where N is the size of the image, $a(x, y)$ is the original object, $b(x, y)$ is the reconstructed image, and maxvalue is the maximum value of the grayscale in the image. The definition of PSNR demonstrates that the greater the PSNR, the better the reconstruction of the image. Through computations, the PSNR value of the B component is obtained as 20.3564, that of the G component as 22.4585, and that of the R component as 22.0929. The obtained PSNR of the colored image is 21.636. Based on the data, a colored image is retrieved accurately and clearly using the proposed scheme.

The scheme is then implemented in an experiment, which are performed in the lab. The setup of the experiment is depicted in Fig. 4. A mode-locked (100 MHz) 355 nm laser is the pump source. The laser is focused into a barium borate (BBO) crystal (type I, noncollinear down conversion). The entangled photon pairs are obtained from the BBO crystal by SPDC. In the experiment, the different sector states are implemented by SLMs, which are reconfigurable diffraction gratings that are used to control the phase structure of light beams to reflect off their surface. A product of Hamamatsu Company, with a screen size of 800 × 600, pixel pitch of 20 μm, and a refresh rate of 60 Hz, is used. The SLMs are parallel-aligned liquid crystal types that modify the phase of light. The entangled photons are then collected via single mode fiber (SMF; 5 μm) to single-photon counter modules (Perkin Elmer). The outputs from the modules are fed to a coincidence counter (made by the authors). The grayscale information of the object in the idler arm is recovered from the different coincidence probabilities in the coincidence counter. Furthermore, a color imaging is obtained in the idler arm through decomposition and synthesis. The spatial resolution and contrast of the images is set by the size of the detection aperture. The single mode fibers in the experimental setup ensure both high resolution and single-mode selectivity.

In theory, the unlimited resolution of the coincidence rate in the simulation will lead to a higher grayscale image of the object. However, the image is constrained to only some grayscales because of the limited coincidence rate in the experiment. A colored "NUPT" image with four grayscales is used for the experiment. In addition, the simulation result of the "NUPT" image is compared with the experimental result.

Each pixel of the three components in the four grayscale objects is encoded with a special phase matrix that corresponds to a $|\theta\rangle$, and these pixels are modulated to the beam. For example, each component is encoded the grayscale "0", "1", "2", and "3", each of which corresponds to the sector states $|\theta{=}0\rangle$, $|\theta = \pi/8\rangle$, $|\theta = \pi/4\rangle$, and $|\theta = \pi/2\rangle$, respectively. Then, each phase matrix is modulated to the beam during the implementation. The simulation and experimental recovery colored images are obtained, shown in Figs. 5(b) and (c), by following the same steps as the simulation experiment. In the simulation, the coincidence rate varies from zero to one; the rate is then normalized to a range of 0 to 255 to calculate the PSNR value. In the experiment, the coincidence counts range from 357 to 1 191; the counts are normalized to a range of 0 to 255 to calculate the PSNR value. Through computations, the mean PSNR of the simulated "NUPT" colored image is determined to be 34.425, whereas the mean experimental result is 8.082. The noise and dark counts in the experiment obviously degrade the PSNR value. However, the experimental results show that the image is clear and recognizable through the proposed scheme. Hence,

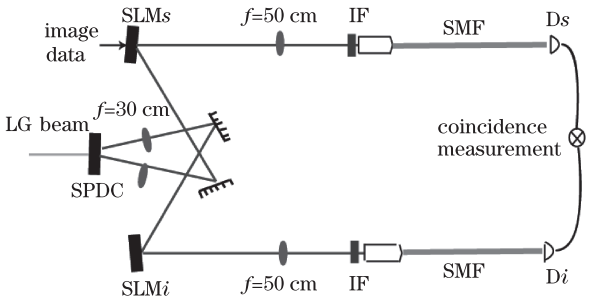

Fig. 4. Schematic of the experimental setup. IF is the interference filter with a 10-nm bandwidth centered at 710 nm.

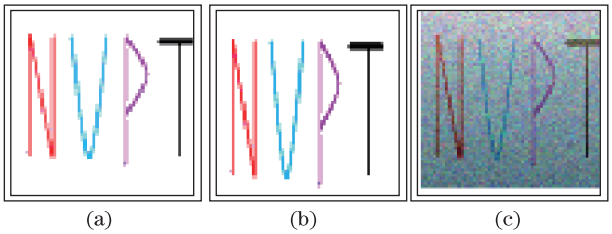

Fig. 5. (a) Original image, (b) simulated image, and (c) reconstructed image from the experiment.

recovering the color of an image using the proposed colored GI scheme is feasible.

In conclusion, we investigate a colored object encoding scheme in the GI system using OAM. We first decompose the colored object into three components (RGB). We then reconstructed the RGB components successively using the encoding scheme with multiple grayscale objects. Lastly, we synthesize the three reconstructed components into a colored image. We implement the scheme through simulations and experiments. The simulation results show that the colored image can be reconstructed clearly with 255 grayscales. The experimental results show the scheme is applicable to colored images with four grayscales. This result shows that recovering the color of an image through the color GI scheme is feasible. The result could expand the use of the GI system to more fields of study because color provides more information from an object.

This work was supported by the National Natural Science Foundation of China (No. 61271238), the Natural Science Research Foundation of Jiangsu Province (No. 11KJA510002), the Open Research Fund Program of the National Laboratory of Solid State Microstructures (Nos. M25020 and M25022), the Foundation for Jiangsu Returned Chinese Scholar (No. NJ210002), the Open Research Fund of the Key Lab of Broadband Wireless Communication and Sensor Network Technology, the Ministry of Education (No. ZD035001NYKL01), the Priority Academic Program Development of Jiangsu Higher Education Institutions, and the Jiangsu Key Laboratory of Image Processing and Image Communication.

References

1. R. Meyers, K. Deacon, and Y. H. Shih, J. Mod. Opt. **54,** 2381 (2007).
2. R. Meyers, K. Deacon, and Y. H. Shih, Phy. Rev. A **77,** 041801(R) (2008).
3. Y. H. Shih, IEEE J. Sel. Top. Quantum Electron. **13,** 1016 (2007).
4. R. S. Bennink, S. J. Bentley, R. W. Boyd, and J. C. Howell, Phys. Rev. Lett. **92,** 033601 (2004).
5. O. Edfors and A. J. Johansson, IEEE Trans. Antennas Propagation **60,** 1126 (2012).
6. T. B. Pittman, Y. H. Shih, D. V. Strekalov, and A. V. Sergienko, Phys. Rev. A **52,** 3429 (1995).
7. A. Gatti, E. Brambilla, M. Bache, and L. A. Lugiato, Phys. Rev. Lett. **93,** 093602 (2004).
8. J. Cheng and S. S. Han, Phys. Rev. Lett. **92,** 093903 (2004).
9. A. Valencia, G. Scarcelli, M. D. Angelo, and Y. H. Shih, Phys. Rev. Lett. **94,** 3601 (2005).
10. F. Ferri, D. Magatti, A. Gatti, M. Bache, E. Brambilla, and L. A. Lugiato, Phys. Rev. Lett. **94,** 3602 (2005).
11. D. Zhang, Y. H. Zhai, L. A. Wu, and X. H. Chen, Opt. Lett. **30,** 2354 (2005).
12. W. L. Gong and S. S. Han, Phys. Rev. A **374,** 1005 (2010).
13. B. Cao, C. Zhang, and P. Ou, Chin. Opt. Lett. **9,** 081102 (2011).
14. B. I. Erkmen and J. H. Shapiro, Adv. Opt. Photon. **2,** 405 (2010).
15. J. H. Shapiro, Phys. Rev. A **78,** 061802 (2008).
16. O. Katz, Y. Bromberg, and Y. Silberberg, Appl. Phys. Lett. **95,** 131110 (2009).
17. F. Ferri, D. Magatti, and L. A. Lugiato, Phys. Rev. Lett. **104,** 253603 (2010).
18. D. Duan and Y. Xia, Chin. Opt. Lett. **10,** 031102 (2012).
19. N. D. Hardy, "Analyzing and improving image quality in reflective ghost imaging", MS. Thesis (Massachusetts Institute of Technology, 2011).
20. B. Jack, J. Leach, J. Romero, S. Franke-Arnold, M. Ritsch-Marte, S. M. Barnett, and M. J. Padgett, Phys. Rev. Lett. **103,** 083602 (2009).
21. S. M. Zhao, J. Ding, X. L. Dong, and B. Y. Zheng, Chin. Phys. Lett. **28,** 124207 (2011).
22. J. Ding and S. M. Zhao, J. NUPT **31,** 2 (2011).
23. S. Franke-Arnold, S. M. Barnett, M. J. Padgett, and L. Allen, Phys. Rev. A **65,** 3823 (2002).
24. H. Li, Z. Chen, J. Xiong and G. H. Zeng, Opt. Express **20,** 2956 (2012).
25. A. Koschan and M. Abidi, *Digital Color Image Processing* (Wiley-Interscience, New Jersey, 2008).
26. J. Leach, B. Jack, J. Romero, M. Ritsch-Marte, R. W. Boyd, A. K. Jha, S. M. Barnett, S. Franke-Arnold, and M. J. Padgett, Opt. Express **17,** 8287 (2009).